Electronic structure and ferromagnetism of Mn-doped group-IV semiconductors

A. Stroppa, S. Picozzi, and A. Continenza
Università degli Studi di L'Aquila, 67010 Coppito (L'Aquila), Italy

A. J. Freeman
Northwestern University, Evanston, Illinois 60208, USA

(Received 23 December 2002; revised manuscript received 30 April 2003; published 8 October 2003)

Accurate *ab initio* full-potential augmented plane wave (FLAPW) electronic calculations within density functional theory in both local density and generalized gradient approximations have been performed for Mn_xGe_{1-x} and Mn_xSi_{1-x} ordered alloys, focusing on their electronic and magnetic properties as a function of the host semiconducting matrix (i.e., Si vs Ge), the Mn concentration, and the spin magnetic alignment (i.e., ferromagnetic vs antiferromagnetic). As expected, Mn is found to be a source of holes and localized magnetic moments of about $3\mu_B$/Mn. The results show that irrespective of the Mn content, the Ge-based systems are very close to half-metallicity, whereas the Si-based structures just miss the half-metallic behavior due to the crossing of the Fermi level by the lowest conduction bands. Moreover, the ferromagnetic alignment is favored compared to the antiferromagnetic one, with its stabilization generally increasing with Mn content; this is in agreement with recent experimental findings for MnGe systems and supports the view that this class of ferromagnetic semiconductors constitute basic spintronic materials.

DOI: 10.1103/PhysRevB.68.155203 PACS number(s): 75.50.Pp, 71.20.Nr

I. INTRODUCTION

The investigation of transition metal impurities in semiconductors has received a great deal of renewed attention in the last few years, due to the enormous potential of room-temperature ferromagnetic diluted magnetic semiconductors (DMSs) as basic materials for spintronic devices.[1–4] In particular, a lot of work has focused on Mn-doped III-V semiconductors, where ferromagnetism has been experimentally observed[2] and theoretically confirmed by electronic structure calculations.[5–8] However, the origin of the ferromagnetism in III-V semiconductors is still a matter of debate, and several different mechanisms (such as the Ruderman-Kittel-Kasuya-Yoshida (RKKY) interaction,[9] double exchange,[10] double resonance,[11] the Zener model,[4] and mean-field theory[12]) have been proposed. Since the early eighties, there has also been a lot of interest in ''traditional'' II-VI DMSs,[13] such as Cd-MnTe, where the Mn solubility is high (at variance with the III-V compounds, where phase segregation is found to occur for Mn concentrations higher than $\sim 8\%$), but which are considered to be less attractive, due to superexchange which favors the antiferromagnetic spin configuration.

On the other hand, group-IV semiconductors (such as Si and Ge) have not been as intensively investigated as III-V or II-VI families, although recently this important class of semiconductors was rediscovered within the spintronics context. In particular, a combined theoretical and experimental work was recently reported for Mn_xGe_{1-x} (Ref. 14); the Curie temperature was found to increase linearly with the Mn concentration up to about 120 K, and the *p*-type semiconducting character and hole-mediated exchange permitted control of the ferromagnetic order through use of a gate voltage of ± 0.5 V. From a theoretical point of view,[14] it was shown that the long-range ferromagnetic interaction dominates the short-range antiferromagnetic exchange.

In this same context, ferromagnetic properties and magnetoresistance phenomena below room temperature have been reported for MnGe, which was partly attributed to Mn_nGe_m ferromagnetic clusters rather than to Mn impurities in the zinc-blende Ge host.[15] Moreover, the discovery of ferromagnetism was reported in highly Mn-doped (up to 6%) Ge single crystals with $T_c = 285$ K,[16] as determined from temperature dependent magnetization and resistance measurements, and a coercive field of 1260 Oe for $x = 0.06$ at 250 K. Finally, Mn ions have been implanted in a Ge matrix[17] and investigated by means of Kerr effect rotation; a magnetic cycle with a coercive field of about 3000 Oe and a hysteresis appearing just below room-temperature were experimentally obtained. Within the theoretical field, the Zener model of carrier-mediated ferromagnetism was used to calculate the Curie temperatures, and a good agreement with experimental data was obtained for III-V materials as a function of Mn concentration[18]; according to this model, the predicted Curie temperatures for *p*-type doped semiconductors with 5% of Mn and 3.5×10^{20} holes/cm^3 are 150 and 75 K for Si and Ge, respectively. Finally, the electronic and magnetic properties of Mn_xGe_{1-x} were studied by accurate first-principles full-potential linearized augmented plane wave (FLAPW) calculations[19] as a function of the Mn positions in a large supercell. The exchange interaction between Mn ions was found to oscillate as a function of the distance between them, obeying an RKKY analytic formula. The estimated Curie temperature[19] ranged from 134 up to 400 K, in good agreement with experiments.[14,16]

Within this framework, we performed first-principles calculations of the electronic and magnetic properties of Mn-doped Si and Ge, using the local spin density approximation to density functional theory (except for one case; see below). Our results, obtained with the highly accurate FLAPW method,[20] show that the ferromagnetic configuration is favored, with all the systems investigated exhibiting a situation very close to half-metallicity. The paper is organized as fol-

TABLE I. Mn concentration (x), number of atoms in the unit cell (N), Bravais vectors ($\mathbf{a_1}, \mathbf{a_2}, \mathbf{a_3}$), and second Mn atom position (the first Mn atom is located in the origin), in internal coordinates.

x	N	$\mathbf{a_1}$	$\mathbf{a_2}$	$\mathbf{a_3}$	Mn pos
0.0625	32	$(a\sqrt{2},0,0)$	$(0,a\sqrt{2},0)$	$(2a,0,0)$	$(\frac{1}{2},\frac{1}{2},\frac{1}{2})$
0.125	16	$(a\sqrt{2},0,0)$	$(0,a\sqrt{2},0)$	$(a,0,0)$	$(\frac{1}{2},\frac{1}{2},0)$
0.25	8	$(a\sqrt{2},0,0)$	$\left(0,\frac{a}{\sqrt{2}},0\right)$	$(a,0,0)$	$(\frac{1}{2},0,0)$
0.50	4	$\left(\frac{a}{\sqrt{2}},0,0\right)$	$\left(0,\frac{a}{\sqrt{2}},0\right)$	$(a,0,0)$	$(\frac{1}{2},\frac{1}{2},\frac{1}{2})$

lows: in Sec. II, we report structural and computational details; in Sec. III, we discuss the most important electronic features in both compounds considering the zinc-blende phase; in Sec. IV, we discuss the structural, electronic, and magnetic properties of a single Mn impurity in a group-IV host, focusing on the difference between Si and Ge; in Sec. V, we determine the effects of the Mn concentration x on the relevant properties of the alloys, in terms of magnetic alignment, magnetic moments and half-metallicity, and in Sec. VI, we draw some conclusions.

II. STRUCTURAL AND COMPUTATIONAL DETAILS

The calculations were performed using the all-electron FLAPW (Ref. 20) method within density functional theory in the local spin density approximation (LSDA).[21] For high transition-metal concentrations, we also considered the generalized gradient approximation (GGA),[22] which is known to affect structural and consequently electronic and magnetic properties.[23] At lower Mn concentrations, however, the LSDA is considered, since it better reproduces the structural properties of pure semiconductors. In the zinc-blende phase, both the GGA and LSDA are considered.

We used a basis set of plane waves with a wave vector up to $K_{max}=3.4$ a.u. and an angular momentum expansion up to $l_{max}=8$ for the potential and the charge density. The muffin-tin radius, R_{MT}, for Mn was chosen equal to 2.4 a.u., while for Si and Ge we used $R_{MT}=1.8$ and 2.0 a.u., respectively. The Brillouin zone sampling was performed using from 6 to 40 special k points according to the Monkhorst-Pack scheme.[24] We carefully checked that these computational parameters were sufficient to accurately determine total energies and magnetic moments within 10–15 meV/Mn and $0.01\mu_B$ (keeping the muffin-tin radii fixed), respectively.

To simulate the alloys, for both the Si- and Ge-based systems, we investigated various concentrations (i.e., $x=0.5$, 0.25, 0.125, 0.0625, and 0.03125) and various different unit cells, having a tetragonal Bravais lattice (except for the zinc-blende phase) and include 32 atoms for the $x=0.0625$ and 0.03125 cases; for higher concentrations, we employed 16, 8, and 4 atoms in the $x=0.125$, 0.25, and 0.5 cases, respectively. A detailed list of the unit cells considered at different concentrations is given in Table I; each contains two Mn impurities in the substitutional site, except for the $x=0.03125$ and the zinc-blende case, where a single Mn impurity occupies the origin of the unit cell. The ferromagnetic (antiferromagnetic) alignment is realized with parallel (antiparallel) magnetic moments on the Mn sites in each cell. The lattice constants are relaxed in the zinc-blende phase, while they are fixed in the other cases at the experimental lattice constant of the host semiconducting matrix,[25] i.e., 10.24 and 10.65 a.u. for Si and Ge, respectively. The internal positions are fully relaxed, according to the calculated *ab initio* atomic forces.

TABLE II. Equilibrium lattice constant a and total magnetic moment μ_{tot} for MnSi and MnGe zinc-blende structures. Also reported are the exchange splittings ($\Delta_x^{t_{2g}}, \Delta_x^{e_g}$) and crystal field splitting (Δ_{CF}), evaluated at Γ, in the GGA calculated MnGe and MnSi band structures.

	a (a.u.)		$\mu_{tot}(\mu_B)$		$\Delta_x^{t_{2g}}$(eV)	$\Delta_x^{e_g}$(eV)	Δ_{CF}(eV)
	LSDA	GGA	LSDA	GGA			
MnSi	9.90	10.29	2.01	2.65	1.5	2.9	1.5
MnGe	10.22	10.69	2.70	3.00	1.8	3.2	1.5

III. MNGE AND MNSI ZINC-BLENDE STRUCTURES

In order to gain insights into the Mn group-IV bonding, we first discuss the $x=50\%$ concentration (MnGe, MnSi) in the zinc-blende structure, where the Mn atom occupies a group-IV site. While such high Mn concentrations cannot be easily reproduced experimentally due to the low solubility of Mn impurities in semiconductors, important aspects of the bonding in a tetrahedral coordination can be extracted from such a study.

We have calculated the MnGe and MnSi total energies vs volume curves for different magnetic alignments, namely antiferromagnetic (AFM), ferromagnetic (FM), and paramagnetic; both GGA and LSDA approximations to density functional theory were considered. Our results for the equilibrium lattice constants, along with the relative total magnetic moments, are reported in Table II. As expected, the magnetic phases are energetically favored more than the paramagnetic one in all cases (at least by 200 meV/Mn). In particular, the FM alignment is the most stable both in the LSDA and GGA. As shown in Table II, the calculated GGA equilibrium lattice constants for both MnSi and MnGe nearly match the constants of the corresponding bulk semiconductor (i.e., Si and Ge, respectively), whereas more significant deviations are present with the local density approximation results.

As far as the electronic properties are concerned, we report in Fig. 1 the GGA calculated MnGe and MnSi band structure at equilibrium. A study of the eigenvalue decomposition into atomic-site-projected wave functions shows that the lower energy region is associated with states having an anion s character, while the states in the energy region between -3.5 and 4.7 eV (in the majority spin channel) and between -1.0 and 5.0 eV (minority spin channel) have mainly a Mn d character. Since each atomic site has a tetrahedral symmetry, the Mn d states are split into t_{2g} (Γ_{15}) and e_g (Γ_{12}) states by the crystal field. The t_{2g} states interact

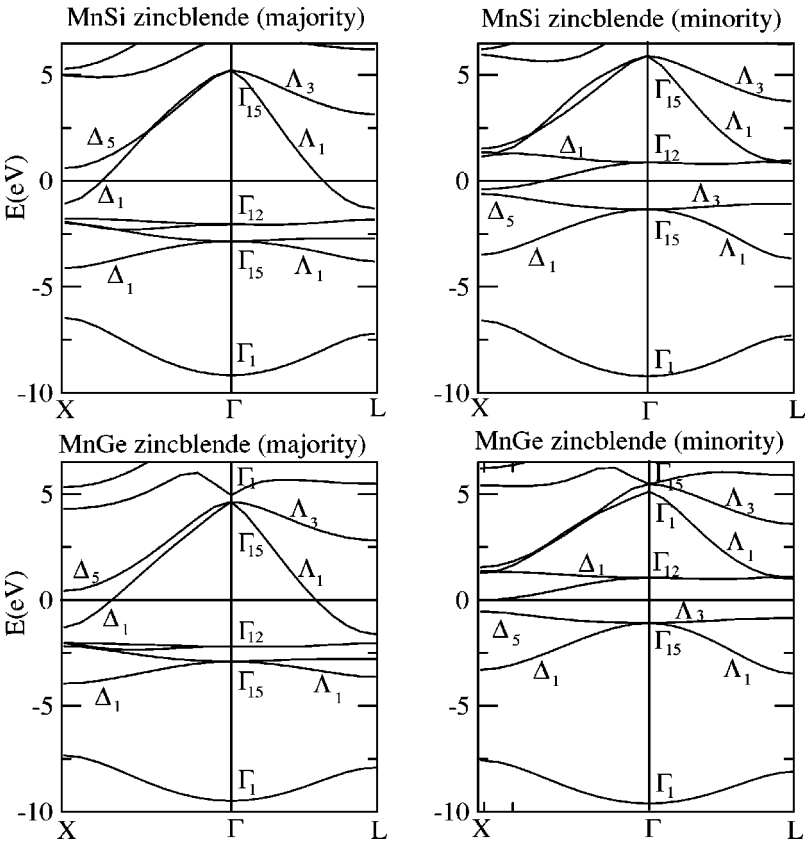

FIG. 1. Majority- and minority-spin band structures for zinc-blende MnGe and MnSi, calculated at equilibrium within the GGA.

with states having the same symmetry from nearest-neighbor atoms, so as to give rise to bonding (t_{2g}^b) and antibonding (t_{2g}^a) levels. On the other hand, the e_g states cannot bond by symmetry and remain more or less unperturbed in the solid compared to the atomic situation. Considering all spin components, we have the following level ordering for both semiconductors: $t_{2g}^+ < e_g^+ < t_{2g}^- < e_g^-$ (where $+/-$ refers to spin-up and -down respectively), called a *high-spin-like* (HSL) level ordering.

In Table II we also report the exchange splittings $\Delta_x^{t_{2g}}$ and $\Delta_x^{e_g}$ and the crystal field splitting (mediated on the spin directions), $\Delta_{e_g - t_{2g}} = \Delta_{CF}$, evaluated at Γ. The electronic band structure has qualitatively the same features in both compounds; there are, however, some important differences. In MnSi, the minority spin e_g band is partially occupied for $\vec{k}$ vectors near X while in MnGe it is completely unoccupied. This is related to two main aspects: (i) the minority e_g level is closer to the Fermi level (set as the zero in the energy scale) in MnSi than in MnGe, and (ii) the dispersion of the minority e_g band is larger in MnSi. These are related to two different aspects: chemical and structural. The different chemical species determine the relative positions of the anion and cation atomic energy levels in the MnSi and MnGe cases, while the different anion size dictates essentially the equilibrium lattice constants. The calculated band structures for both MnSi and MnGe at the same lattice constant show very similar features and we find that the half-metallicity is lost in MnGe if we constrain it at the MnSi equilibrium volume. Both chemical and structural effects lead to a greater hybridization (higher e_g band dispersion) in MnSi, which is in part responsible for the loss of the half-metallicity.

IV. MN IMPURITY IN A GROUP-IV MATRIX: SI VS GE

In Table III we report, the FLAPW calculated relevant properties of the Mn impurity in a Si and Ge matrix (i.e., one Mn atom in a 32-atom cell), namely, formation energies, relevant bond lengths, and magnetic moments. Recall that in this configuration, the Mn atoms are forced to be ferromagnetically aligned; the paramagnetic state was also considered, but the resulting total energy for Mn:Si was found to be about 390 meV higher than the FM spin configuration, in agreement with the experimental magnetic state of Mn_xGe_{1-x} alloys.[14] Therefore, in the following, we focus only on the FM and AFM alignments.

Let us first examine the formation energies, evaluated as in Ref. 26 and taking as reference for the Mn chemical potential the value in the AFM [001]-ordered fcc lattice. The

TABLE III. FLAPW calculated relevant properties in $Mn_{0.03125}Si_{0.96875}$ and $Mn_{0.03125}Ge_{0.96875}$: formation energies E_f (eV), nearest neighbor bond length d^{Mn-IV} (a.u.), total magnetic moment μ_{tot} (in μ_B), Mn magnetic moment μ_{Mn} (in μ_B), and nearest neighbor group-IV magnetic moment $\mu_{IV_{n.n.}}$ (in μ_B).

	E_f	d^{Mn-IV}	μ_{tot}	μ_{Mn}	$\mu_{IV_{n.n.}}$
$Mn_{0.03125}Si_{0.96875}$	2.3	4.43	2.99	2.83	−0.03
$Mn_{0.03125}Ge_{0.96875}$	1.5	4.55	3.00	3.10	−0.04

relatively high formation energies of a Mn defect in a group-IV matrix suggests that, similar to the case of III-V semiconductors, a high level of Mn concentration could cause a clustering of Mn atoms and/or the formation of undesired Mn-IV compounds[15] (such as $Mn_{11}Ge_8$ or Mn_2Ge_5), rather than a Mn_xIV_{1-x} alloy in which Mn impurities randomly substitute the group-IV atom in a zinc-blende-like ordering. The formation energy shown in Table III is higher in the Si matrix than in the Ge matrix; this may be due to size-related effects. In fact, the Mn atom belongs to the same row of the Periodic Table as Ge, so we might expect the introduction of Mn to be less expensive energetically in a Ge matrix compared to a Si matrix.

The Mn-Ge and Mn-Si bond lengths are more or less unaltered compared to their respective bulk group-IV bond lengths (the deviations are at most 1.7%). This is in agreement with the results of Park *et al.*[14] In their work, the internal relaxations were not considered due to negligible forces acting on the Mn atom substituting Ge sites. For the discussion of the electronic and magnetic properties, it is helpful to look at the density of states (DOS) of the MnSi [Fig. 2(a)] and MnGe [Fig. 2(b)] systems. A comparison between the total DOS with and without the impurity shows that far from the Fermi level E_F, the DOS remains close to that of the host matrix DOS, since the effect of Mn is evident only starting at about -4 eV below E_F (set as zero of the energy scale); in particular, the most affected component in the valence region is the spin-up part. In the region between -1 and 2 eV, the perturbation is evident for both spin components. In particular, the hybridization between Mn and the group-IV atom results in states in proximity to E_F and, in particular, in the energy gap region of the semiconductor.

Further insights can be gained from the Mn *d* partial DOS [see the shadowed region in Figs. 2(a) and 2(b)]. An analysis of the eigenvalue decomposition shows the following. (i) In the spin-up part, the main peak (centered at about -2.3 eV in both Si and Ge hosts) corresponds to both e_g and t_{2g}^b levels, whereas the feature around E_F has a t_{2g}^a character, with these states only partially occupied. (ii) In the spin-down part, the peak centered at about -1 eV corresponds to t_{2g}^b states, whereas the well-localized peak at about 0.5 eV above E_F has an e_g origin and the features at around 1 eV have t_{2g}^a character. It is therefore evident that the spin-down (spin-up) bands are mostly unoccupied (occupied); this results in the total magnetic moment being close to $3\mu_\beta$ in both compounds, which is mostly localized on Mn (see Table III). Furthermore, an estimate of the crystal field splitting, $\Delta_{e_g-t_{2g}}$, and exchange splitting, Δ_x, for the e_g state in the Ge (Si) case leads to 1.4 and 2.7 eV (1.2 and 2.4 eV), respectively. These values are nearly the same as those relative to the zinc-blende case.

The integer total magnetic moment (see Table III) suggests MnGe to be a half-metallic compound, whereas MnSi is ''close'' to half-metallicity. This behavior is clearly evident in the total DOS shown in Figs. 2(a) and 2(b): in the Ge case, the DOS shows a valley around E_F and is strictly zero at E_F in the minority spin channel; on the other hand, this same valley is still present in the Si case, but is located just below

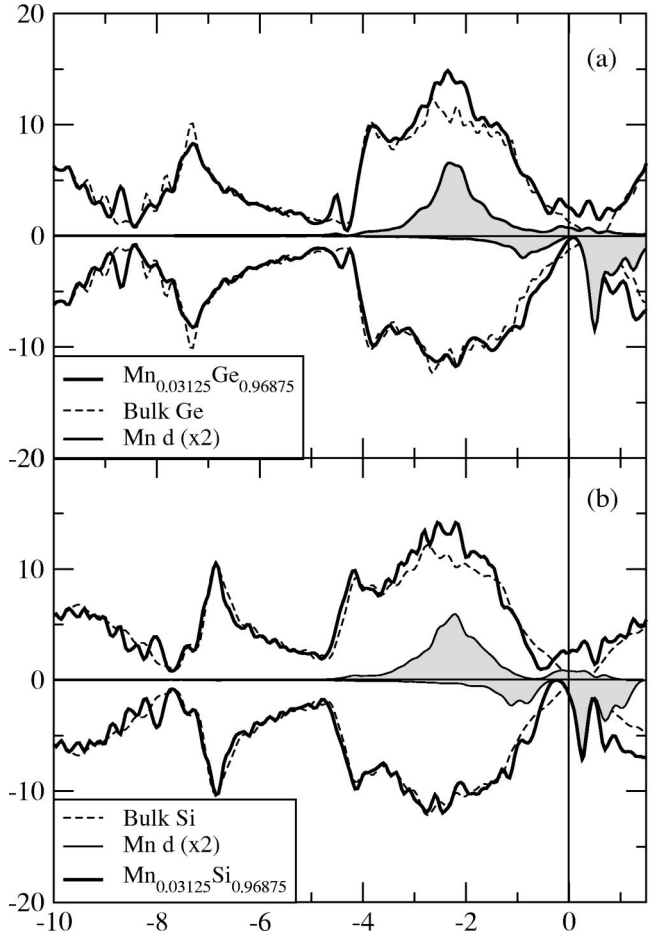

FIG. 2. (a) Total DOS (bold line) for FM $Mn_{0.03125}Ge_{0.96875}$, bulk Ge total DOS (dashed line), and Mn *d* PDOS (solid line—shaded region). (b) Total DOS (bold line) for FM $Mn_{0.03125}Si_{0.96875}$, bulk Si total DOS (dashed line), and Mn *d* PDOS (solid line—shaded region). To demonstrate more clearly the role of the magnetic impurity in the plot, the Mn 3*d* PDOS is multiplied by a factor of 2. The total DOSs with and without Mn are aligned in energy by shifting the semiconducting DOS so as to make the core levels coincident with a core level of a group-IV atom far from the impurity.

E_F (see the discussion in Sec. III) so that the spin-down DOS at E_F is finite. A comparison between the Mn *d* partial density of states (PDOS) in the two systems also explains the smaller Mn magnetic moment in the Si case; the upper DOS is more or less unaltered, giving rise to a very similar integral [i.e., same spin-up charge within the muffin tin (MT) sphere]. On the other hand, the integral of the spin-down DOS (i.e., spin-down charge within the MT sphere) is larger in the Si case (by about 0.2 electrons), and so the final magnetic moment is larger in the Ge case. This difference is related to the states in proximity to E_F: as shown in the high concentration limit (50%), the larger hybridization occurring in Si makes some of the e_g-like states lying close to E_F occupied.

The band structure of the diluted systems is shown in Fig. 3. The lower energy region, between ~ -12 eV and ~ -5 eV (not shown), has mainly a group-IV *s* character, fol-

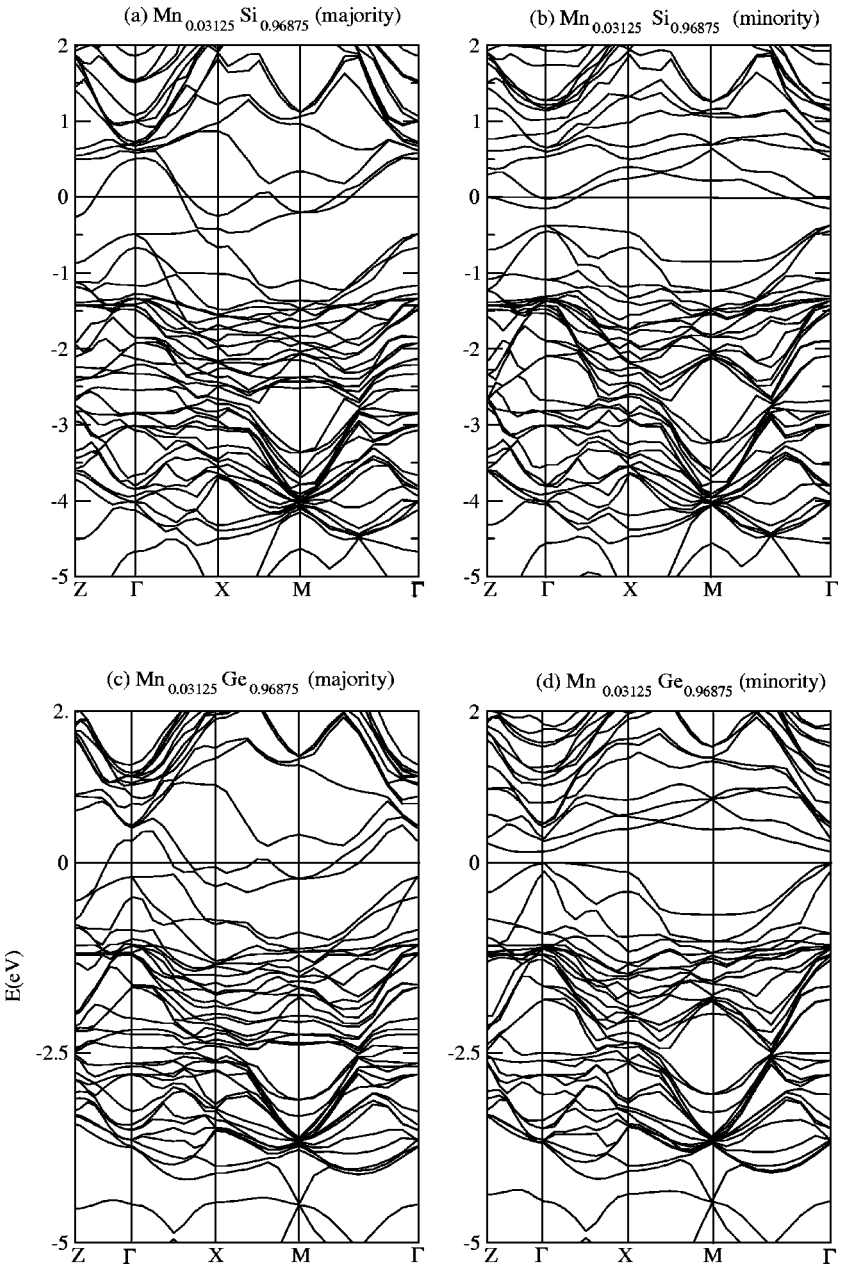

FIG. 3. (a) Majority-spin and (b) minority-spin band structures for FM $Mn_{0.03125}Ge_{0.96875}$. (c) Majority-spin and (d) minority-spin band structures for FM $Mn_{0.03125}Si_{0.96875}$.

lows the expected trend in energy (i.e., the binding energy of Ge 4*s* states are higher than those of Si 3*s* states), and is basically unaffected by the exchange splitting of Mn *d* states. The character of the bands in the energy range shown is mainly of Mn *d* and group-IV *p*. As far as the half-metallicity is concerned, the valence band maximum of the minority spin channel in MnGe [see Fig. 3(d)] reaches E_F at Γ, so that the spin gap (i.e., the minimum energy required to flip the electron spin) is zero; on the other hand, the energy gap is indirect (since the lowest conduction energy level is along the Γ-*Z* line) and is about 0.14 eV. The bands around E_F in the majority spin channel arise from Mn *d* and Ge *p* hybridizations, so as to give rise to hole pockets close to Γ. The band structure of MnSi [see Figs. 3(a) and 3(b)] is qualitatively similar to the MnGe case, except that E_F intercepts energy bands in both the up- and down-spin channels so that the half-metallicity is lost and the behavior is metallic.

As seen in Fig. 4(a), in Mn:Ge the spin-density contour plots show that the spin magnetic moments are essentially localized around the Mn atom (as is also evident from Table III) and the polarization induced on the nearest-neighbor atom (Si or Ge) is negative. Moreover, the spin density spatial distribution along the nearest-neighbor Ge bonds reveals its *p* character. This is believed to be a signature of the AFM coupling between the polarized hole and the Mn spin in the model proposed by Zener[4] to explain DMS ferromagnetism. It was also suggested[6] that in Mn-doped magnetic semiconductors, the antiferromagnetic interaction between Mn 3*d* and its nearest-neighbor anion *p* states could lower the total energy, therefore stabilizing the ferromagnetic alignment. This is consistent with our present findings. In addition, a careful inspection of the magnetic moments induced on the group-IV atoms shows an oscillatory and decreasing trend as a function of the distance from the Mn impurity [see Fig.

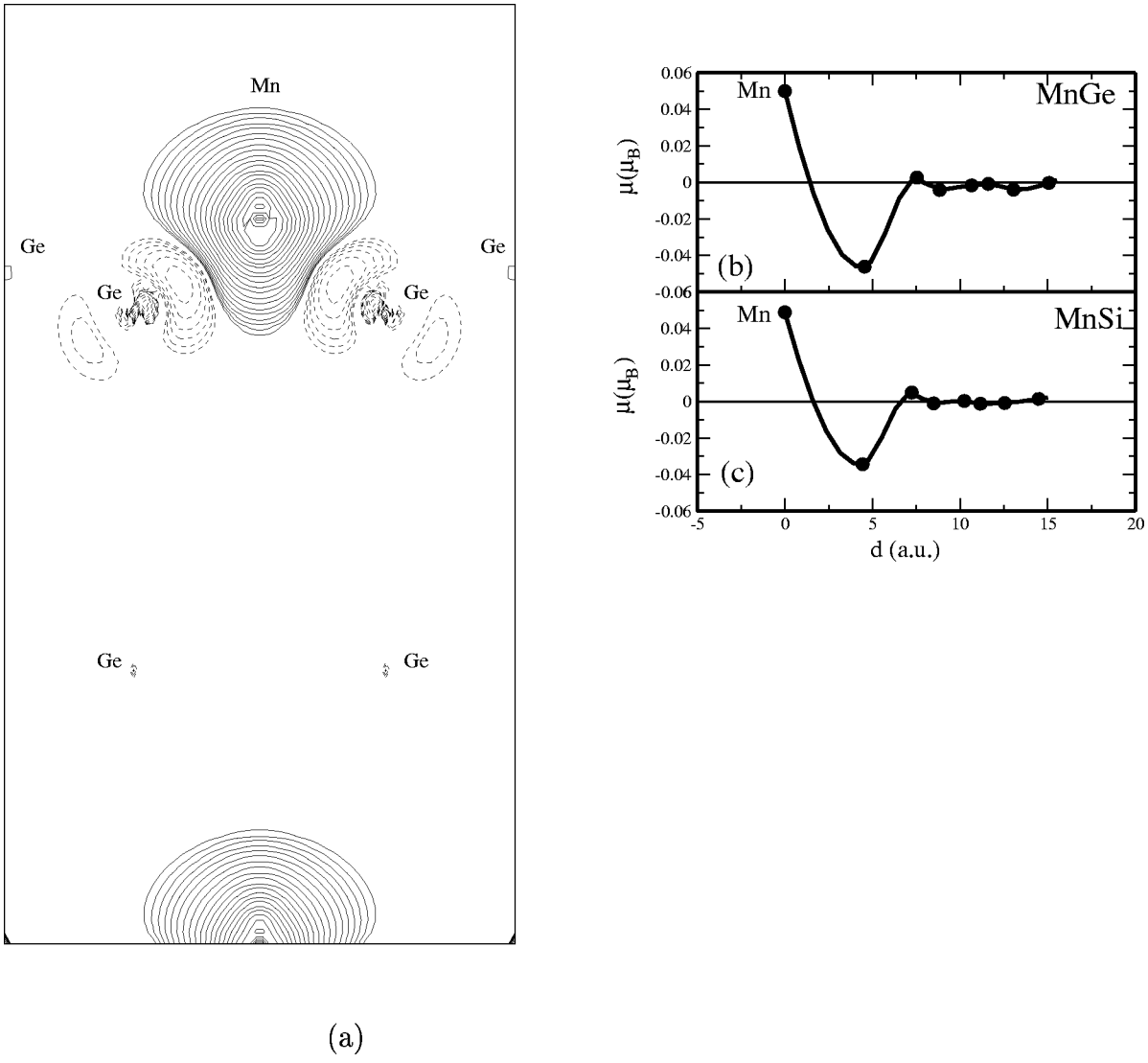

FIG. 4. (a) Spin density for $Mn_{0.03125}Ge_{0.96875}$ in the [110] plane. Spin density contours start at $1\times10^{-3}e^{-}$/cell and increase successively by a factor of $2^{1/2}e^{-}$/cell. The positive (negative) spin density is shown by solid (dashed) lines. (b) Induced Si magnetic moments (in μ_B) vs distance from the Mn atom. (c) Induced Ge magnetic moments (in μ_B) vs distance from Mn.

4(b)]. This oscillatory trend is more evident for the *s* rather than the *p* polarization. Overall, the group-IV atoms have but a negligible polarization, giving further evidence of the strongly localized nature of the magnetism in DMSs.

V. HIGHER MN CONCENTRATION IN A GROUP-IV MATRIX

In Fig. 5, we plot the relevant properties, such as total energies and magnetic moments, as a function of the Mn concentration. Let us first focus on the difference of total energies, $\Delta_{FA}=E_{AFM}-E_{FM}$, between the AFM and ferromagnetic (FM) spin configurations, shown in Fig. 5(a), for both Mn_xGe_{1-x} and Mn_xSi_{1-x}. It is remarkable that all structures show the FM alignment as the favored spin alignment; this is in agreement with the experimentally observed ferromagnetic state in Mn_xGe_{1-x} alloys and therefore suggests these systems as a new class of ferromagnetic semiconductors, to be used as basic materials in spintronic devices. These findings are in agreement with those obtained by Zhao *et al.*,[19] which found that the Mn-Mn magnetic coupling is strongly dependent on the overall Mn distribution in the environment and that the FM coupling is always energetically very competitive. Moreover, Si and Ge hosts show very similar behaviors; in particular, Δ_{FA} is more or less unaltered for the two lowest concentrations, whereas some differences, though small, show up in the high concentration limit: the Ge-based structures seem to favor FM alignment more than the Si-based alloys do. Furthermore, as a general trend, Δ_{FA} increases with Mn concentration; however, the tendency towards FM alignment is clearly evident even for the lowest concentration examined (i.e., $x=0.0625$, which is of the same order of magnitude as that achieved in experimental samples), namely, Δ_{FA} is of the order of 100 meV/Mn. The trend in Δ_{FA} with x is consistent with the increase of the Curie temperature with Mn concentration observed in Mn_xGe_{1-x} alloys.[14]

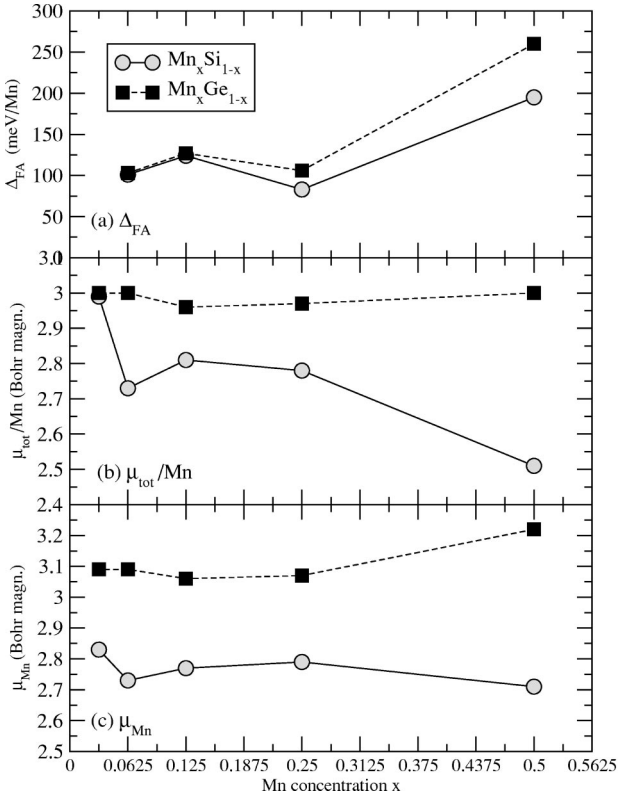

FIG. 5. (a) Difference between total energies in the AFM and FM configurations, (b) total magnetic moment per Mn atom (in μ_B), and (c) Mn magnetic moments in the muffin tin sphere (in μ_B) for Mn_xSi_{1-x} (squares and dashed line) and Mn_xGe_{1-x} (circles and solid line).

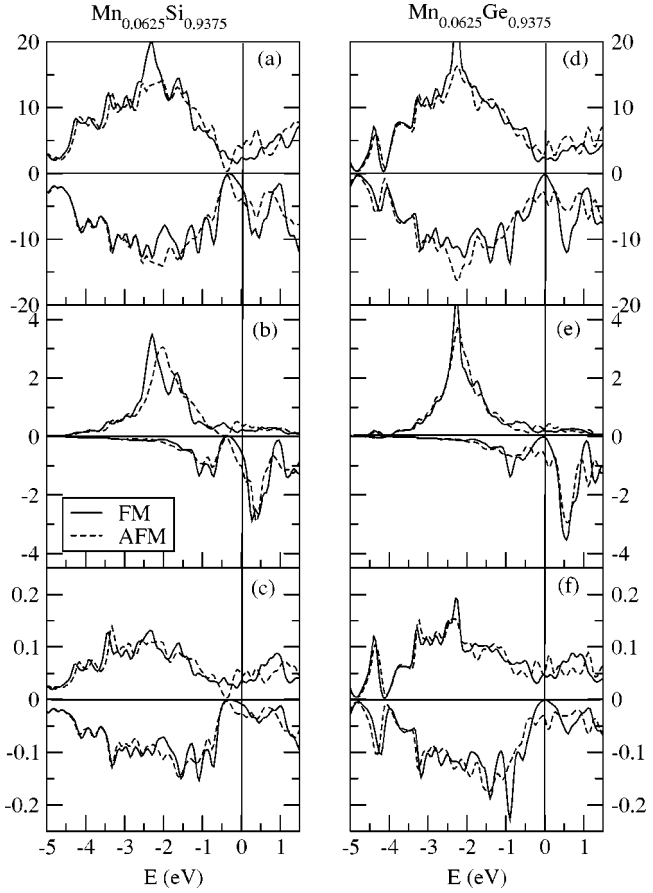

FIG. 6. DOS for $Mn_{0.0625}Si_{0.9375}$: (a) Total, (b) Mn *d* PDOS, (c) Si PDOS, (d) total, (e) Mn *d* PDOS, and (f) Ge PDOS. The solid (dashed) lines show the FM (AFM) spin configuration.

As for the trends of the total magnetic moments shown in Fig. 5(b) only for the FM spin alignment, we note that the MnGe systems tend to keep a total magnetic moment close to $3\mu_B$ (i.e., consistent with the half-metallic behavior shown by the DOS), irrespective of the Mn content. On the other hand, the MnSi systems are more sensitive to *x*, showing in particular an increasing tendency towards half-metallicity as the Mn concentration is reduced.

Finally, we discuss the trends of the Mn magnetic moment, μ_{Mn}, as a function of *x*, shown in Fig. 5(c). First of all, the magnetic moment is essentially of $3d$ origin, since the $4s$ and $4p$ spin polarizations are very weak. It is remarkable that the Mn total charge and total *d* electron population in the muffin-tin sphere are about $6e^-$ and $5.85e^-$ ($5.2e^-$ and $5.15e^-$) in the MnGe (MnSi) alloys, respectively, for all concentrations. This is consistent with what was already pointed out in the MnGaAs case:[6] since the *d* population is higher than in the Mn free atom, there could be a population inversion, i.e., an $s \rightarrow d$ promotion, in marked contrast with the Ludwig-Woodbury model.[27] The relevant feature of Fig. 5(c) is that neither MnSi nor MnGe show a definite (i.e., increasing or decreasing) trend with Mn content, but rather a very similar value is kept for all concentrations. This confirms that, as noticed when discussing the spin density, the Mn magnetic moment is to a large extent determined by local effects, i.e., by the four nearest neighbors (tetrahedrally coordinated at a fixed distance). The critical distance and the anion chemical species are, on the other hand, relevant in determining the Mn magnetic moment within the Mn muffin-tin sphere (with a radius kept equal in the Si and Ge cases): it is clear from Fig. 5(c) that μ_{Mn} is larger for the Ge (about $3.1\mu_B$) compared to the Si host matrix (about $2.75\mu_B$). As already discussed, this is due to both chemical and size effects: in fact, we find a larger *p-d* hybridization in the case of Si compared to Ge, and a resulting reduction of the Mn magnetic moment compared to the ideal atomic value.

As a final remark, we point out that the exchange-correlation parametrization (i.e., LSDA vs GGA) does not play a crucial role. Tests performed for the $Mn_{0.125}Si_{0.875}$ case within both parametrizations show that both the total and Mn magnetic moments are larger by about $0.1\mu_B$ within the GGA compared to the LSDA. However, this small change does not alter the half-metallic vs metallic character of the system: for MnSi (with $x \leqslant 0.0625$), half-metallicity is lost both within the LSDA and GGA.

In Fig. 6 we show the DOS in the AFM and FM configurations for $x = 0.0625$ in both Si and Ge. A comparison between the total DOS shows that in the Ge case the behavior is dramatically changed by the magnetic alignment: the half-metallic character of the FM spin configuration is lost, since the AFM configuration shows a metallic behavior, due to the introduction of states at E_F. A similar mechanism acts in the

TABLE IV. FLAPW calculated magnetic moments in Mn_xSi_{1-x} and Mn_xGe_{1-x} as a function of Mn concentration x in FM and AFM spin configurations: Mn magnetic moment μ_{Mn} (in μ_B), and nearest neighbor magnetic moment ($\mu_{Si_{n.n.}}$ and $\mu_{Ge_{n.n.}}$) (in μ_B).

	$Si_{0.9375}Mn_{0.0625}$		$Si_{0.875}Mn_{0.125}$		$Si_{0.75}Mn_{0.25}$		$Si_{0.5}Mn_{0.5}$	
	FM	AFM	FM	AFM	FM	AFM	FM	AFM
μ_{Mn}	2.73	± 2.59	2.77	± 2.56	2.77	± 2.54	2.71	± 2.39
$\mu_{Si_{n.n.}}$	-0.03	∓ 0.03	-0.03	∓ 0.03	-0.06	∓ 0.06	-0.12	0
	$Ge_{0.9375}Mn_{0.0625}$		$Ge_{0.875}Mn_{0.125}$		$Ge_{0.75}Mn_{0.25}$		$Ge_{0.5}Mn_{0.5}$	
	FM	AFM	FM	AFM	FM	AFM	FM	AFM
μ_{Mn}	3.09	± 3.02	3.06	± 2.99	3.07	± 2.97	3.22	± 2.89
$\mu_{Ge_{n.n.}}$	-0.05	∓ 0.04	-0.05	∓ 0.04	-0.09	∓ 0.09	-0.17	0

Si case, so that there is a filling of states in the valley in proximity to E_F; however, the resulting effects are relatively less important compared to Ge, since some states at E_F were already present in the FM case, so that the overall metallic behavior is not changed.

The Mn *d* PDOS shows similar features in the FM and AFM cases, consistent with their very similar magnetic moment values. This suggests that the magnetic moments in these diluted semiconducting systems are well localized. In Figs. 6(c) and 6(f) we show the PDOS relative to the group-IV atom that is the nearest neighbor of Mn. It is evident that anion states (essentially of *p* origin) strongly hybridize with Mn *d* states, resulting in an induced spin polarization.

The Mn and IV magnetic moments as a function of concentration are reported in Table IV for the FM and AFM spin configurations. What was pointed out when discussing Fig. 6, namely, (i) the slightly negative spin polarization of the group-IV nearest neighbor atoms, and (ii) the similarity between the Mn and group-IV magnetic moments in FM and AFM spin configurations (even with a relatively high concentration of magnetic impurities, $x \leqslant 0.25$), is basically unaffected by the Mn content, showing once more that the relevant magnetic properties are determined locally.

VI. CONCLUSIONS

Accurate FLAPW calculations have been performed within the local density approximation and the GGA to density functional theory for MnGe and MnSi systems, focusing on the effects of (i) the host matrix (i.e., Si vs Ge), (ii) the Mn content, and (iii) the spin magnetic alignment (i.e., FM vs AFM) on the relevant electronic and magnetic properties. Common to other DMSs, Mn is found to stabilize a magnetic state (compared to the paramagnetic one), being a source of hole pockets and of localized magnetic moments of about $3\mu_B$. We were able to show that due to a lower degree of hybridization, half-metallicity is found for the Ge-based systems, whereas it is just missed when Mn-doped Si. Moreover, our results indicate a stable FM alignment in all the systems investigated in both Si- and Ge-based structures, with Δ_{FA} increasing with the magnetic impurity concentration. These findings are in agreement with the experimental observation of a stable Mn_xGe_{1-x} ferromagnetic semiconductor, with a Curie temperature increasing with the Mn content. Based on our results and on recent experiments,[14,16,17] the use of these materials in potentially new spin-based devices is suggested; in particular, the 100% spin polarization of the carriers and the stronger stability of the FM spin configuration compared to the AFM configurations seem to suggest Ge-based structures as more promising within the spintronics framework.

ACKNOWLEDGMENTS

We acknowledge support by INFM through Iniziativa Trasversale Calcolo Parallelo. The Work at Northwestern University was supported by Darpa/ONR Grant No. N00014-02-1-0887.

[1] H. Ohno, Science **281**, 951 (1998).
[2] Y. Ohno, D.K. Young, B. Beschoten, F. Matsukura, H. Ohno, and D.D. Awschalom, Nature (London) **402**, 790 (1999).
[3] R. Fiederling, M. Keim, G. Reuscher, W. Ossau, G. Schmidt, A. Waag, and L.W. Molenkamp, Nature (London) **402**, 787 (1999).
[4] T. Dietl, H. Ohno, F. Matsukura, J. Cibert, and D. Ferrand, Science **287**, 1019 (2000).
[5] S. Sanvito, P. Ordejon, and N.A. Hill, Phys. Rev. B **63**, 165206 (2001).
[6] Y.J. Zhao, W.T. Geng, K.T. Park, and A.J. Freeman, Phys. Rev. B **64**, 035207 (2001).
[7] M. Jain, L. Kronik, J.R. Chelikowski, and V.V. Godlevsky, Phys. Rev. B **64**, 245205 (2001).
[8] M. van Schilfgaarde and O.N. Mryasov, Phys. Rev. B **63**, 233205 (2001).
[9] F. Matsukura, H. Ohno, A. Shen, and Y. Sugawara, Phys. Rev. B **57**, R2037 (1998).
[10] H. Akai, Phys. Rev. Lett. **81**, 3002 (1998).

[11] J. Inoue, S. Nonoyama, and H. Itoh, Phys. Rev. Lett. **85**, 4610 (2000).
[12] M. Yagi, K. Noba, and Y. Kayanuma, J. Lumin. **94-95**, 523 (2001).
[13] A. Haury, A. Wasiela, A. Arnoult, J. Cibert, S. Tatarenko, T. Dietl, and Y. Merlè d'Aubigné, Phys. Rev. Lett. **79**, 511 (1997); D. Ferrand *et al.* J. Cryst. Growth **214/215**, 387 (2000).
[14] Y.D. Park, A.T. Hanbicki, S.C. Erwin, C.S. Hellberg, J.M. Sullivan, J.E. Mattson, T.F. Ambrose, A. Wilson, G. Spanos, and B.T. Jonker, Science **295**, 651 (2002).
[15] Y.D. Park, A. Wilson, A.T. Hanbicki, J.E. Mattson, T. Ambrose, G. Spanos, and B.T. Jonker, Appl. Phys. Lett. **78**, 2739 (2001).
[16] Y. Kim, S. Cho, S.Y. Choi, S.C. Hong, Bong-Jum Kim, J.H. Jung, Y.C. Kim, and J.B. Ketterson, Phys. Rev. B **66**, 033303 (2002).
[17] F. D'Orazio, F. Lucari, M. Passacantando, S. Picozzi, S. Santucci, and A. Verna, IEEE Trans. Magn. **38**, 2856 (2002).
[18] T. Dietl and H. Ohno, Physica E **9**, 185 (2001).
[19] Y.J. Zhao, T. Shishido, and A.J. Freeman, Phys. Rev. Lett. **90**, 047204 (2003).
[20] E. Wimmer, H. Krakauer, M. Weinert, and A.J. Freeman, Phys. Rev. B **24**, 864 (1981); H.J.F. Jansen and A.J. Freeman, *ibid.* **30**, 561 (1984).
[21] U. von Barth and L. Hedin, J. Phys. C **5**, 1629 (1972).
[22] J.P. Perdew, K. Burke, and M. Ernzerhof, Phys. Rev. Lett. **77**, 3865 (1996).
[23] A. Continenza, S. Picozzi, W.T. Geng, and A.J. Freeman, Phys. Rev. B **64**, 085204 (2001).
[24] H.J. Monkhorst and J.D. Pack, Phys. Rev. B **13**, 5188 (1976).
[25] Walter Harrison, *Electronic Structure and the Properties of Solids* (W.H. Freeman & Co., San Francisco, 1980), p. 175.
[26] S.B. Zhang, S.H. Wei, A. Zunger, and H. Katayama-Yoshida, Phys. Rev. B **57**, 9642 (1998); S.H. Wei, S.B. Zhang, and A. Zunger, J. Appl. Phys. **85**, 7214 (1999).
[27] G.W. Ludwig and H.H. Woodbury, in *Solid State Physics*, edited by H. Ehrenreich, F. Seitz, and D. Turnbull (Academic, New York, 1962), Vol. 13, p. 223.